Magnetic Resonance in Medicine 59:1347–1354 (2008)

AxCaliber: A Method for Measuring Axon Diameter Distribution from Diffusion MRI

Yaniv Assaf,[1*] Tamar Blumenfeld-Katzir,[1] Yossi Yovel,[1] and Peter J. Basser[2]

The diameter of a myelinated nerve axon is directly proportional to its conduction velocity, so the axon diameter distribution helps determine the channel capacity of nervous transmission along fascicles in the central (CNS) and peripheral nervous systems (PNS). Previously, this histological information could only be obtained using invasive tissue biopsies. Here we propose a new NMR-based approach that employs a model of water diffusion within "restricted" cylindrical axons to estimate their diameter distribution within a nerve bundle. This approach can be combined with MRI to furnish an estimate of the axon diameter distribution within each voxel. This method is validated by comparing the diameter distributions measured using the NMR and histological techniques on sciatic and optic nerve tissue specimens. The axon diameter distribution measured in each voxel of porcine spinal cord using MRI and using histological methods were similar. Applications are expected in longitudinal studies designed to follow nerve growth in normal and abnormal development, as well as in diagnosing disorders and diseases affecting specific populations of axons in the CNS and PNS. Magn Reson Med 59:1347–1354, 2008. © 2008 Wiley-Liss, Inc.

Key words: axon diameter; diffusion; MRI; nerve; q-space

Axon diameter directly affects nerve function. It is well known that in myelinated axons, nerve conduction velocity is directly proportional to axon diameter (1–4). Thus, large-diameter axons generally arise in neuronal pathways that need fast reaction times (e.g., in motor pathways) while smaller axons arise in neuronal pathways that permit slower reactions (e.g., pain and temperature control). The latency of action potentials is also known to affect the nervous system function through mechanisms of temporal summation (5,6). Clearly, axon diameter is also a determinant of latency through its effect on conduction velocity. Finally, axon diameter affects the current magnitude and downstream synaptic branching pattern (7).

Owing to its critical functional role in the central (CNS) and peripheral nervous systems (PNS) axon diameter distribution is an important quantity to measure in different nerve pathways both in normal and abnormal development and in health and disease. For instance, it is hypothesized that in amyotrophic lateral sclerosis (ALS) large diameter axons (type A-alpha) are damaged selectively (8,9), while in autism small-diameter axons are maldeveloped (10).

Despite its importance, the axon diameter distribution within nerve fascicles has not been measurable in vivo, and currently can only be assessed by invasive histological means. Generally, electron microscopy can provide the axon diameter distribution, but only of a limited area of a tissue section. The tissue preparation and morphometric analysis are difficult and in many cases tedious, and the results are subject to many well-known artifacts, including tissue disintegration, tissue shrinkage and cracking, nonuniform staining, and statistical bias owing to the fact that only a small amount of tissue is sampled.

Here we propose a noninvasive, in vivo methodology for measuring the axon diameter distribution, which is based on diffusion NMR and MRI data. Diffusion MR currently provides unique information about the macroscopic organization of white matter (11–20). In particular, diffusion tensor imaging (DTI) has become the leading method for analysis of neuronal fiber pathways and their visualization (tractography) (21–25). Contrast in diffusion MR arises from signal loss caused by the displacement of water molecules, which is described statistically by a displacement probability distribution (13,15,26,27). DTI assumes a Gaussian displacement distribution that adequately accounts for the differences in diffusivity measured along different directions (anisotropy) in neuronal fibers (13,15). While parallel to axon bundles water diffusion is relatively free; perpendicular to them it is hindered (11–19). However, several years ago it was found that the Gaussian displacement distribution is not adequate to describe the pool of water that is restricted or trapped within the intra-axonal space (when measured perpendicular to the fibers) (28,29).

The non-Gaussian nature of water diffusion within axons provides a unique opportunity to estimate microstructural features of nerve axons not accessible with DTI (28). By assuming that white matter can be represented by a polydisperse array of closely packed impermeable cylinders, one can adapt MR-based methodologies originally developed in the porous media field (30,31) to estimate quantities such as the axon diameter distribution and the volume fraction of intra-axonal space. Specifically, these MR methods build on models of restricted diffusion within pores originally proposed by Stejskal and Tanner, and then further developed by Packer and others for applications in materials and food sciences (26,32–35). The possibility of combining these pore structure characterization measurements with MRI was facilitated by the development of the q-space concept, introduced by Cory and

[1]Department of Neurobiology, the George S. Wise Faculty of Life Sciences, Tel Aviv University, Tel Aviv, Israel.

[2]Section on Tissue Biophysics and Biomimetics, Laboratory of Integrated Medical Biophysics, National Institute of Child Health and Human Development, National Institutes of Health, Bethesda, Maryland, USA.

Grant sponsor: Intramural Research Program of the National Institute of Child Health and Human Development, NIH (to P.J.B.); Grant sponsor: Adams Super Center for Brain Studies at Tel Aviv University (to Y.A.); Grant sponsor: Ministry of Science of the State of Israel (Tashtiot Program) (to Y.A.); Grant sponsor: Israel Science Foundation (ISF) (to Y.A.).

*Correspondence to: Dr. Yaniv Assaf, Department of Neurobiochemistry, Faculty of Life Sciences, Tel Aviv University, Tel Aviv, 69978, Israel. E-mail: asafyan@zahav.net.il

Received 31 July 2007; revised 18 December 2007; accepted 8 January 2008.

DOI 10.1002/mrm.21577

Published online in Wiley InterScience (www.interscience.wiley.com).

© 2008 Wiley-Liss, Inc.

Callaghan in the early 1990s and 3D q-space MRI (QSI) originally proposed by Callaghan (30,31).

The framework used in this article models nerve white matter as a composite medium, consisting of an extra-axonal space in which water diffusion is hindered, but not restricted, and distinct intra-axonal spaces in which water is trapped or restricted. Previously, we referred to this experimental and modeling paradigm as CHARMED, which stands for composite hindered and restricted model of diffusion (36,37).

Here we extend the CHARMED framework by introducing the diameter distribution of restricted cylindrical axons as an unknown function to estimate using diffusion MR data having both different degrees of diffusion weighting and different diffusion times. We call this new modeling and experimental approach *AxCaliber*.

The AxCaliber framework can be applied spectroscopically, i.e., treating an entire specimen as one homogeneous voxel, or in combination with MRI, in which the axon diameter distribution can be measured within particular voxels in an imaging volume. We validate AxCaliber NMR using a fixed porcine optic and sciatic nerve specimen, and AxCaliber MRI using a fixed porcine spinal cord specimen on a pixel-by-pixel basis. This imaging information is further used to determine whether it is possible to segment the spinal cord into different and distinct regions, each having similar diameter distributions, consistent with the known somatotopic organization of their neuronal pathways.

MATERIALS AND METHODS

Samples

Experiments were performed on formalin-fixed tissue samples of porcine sciatic and optic nerves ($n = 5$ each) and porcine spinal cord (at the lower cervical level) ($n = 4$). The tissue was excised and immediately immersed in 4% formalin for at least 48 hr before the experiment. Prior to the MRI acquisition, samples were placed in buffered saline for rehydration and following the MRI placed back in 4% formalin. Then the samples were prepared for histology (electron microscopy for the nerves and histochemistry staining for the spinal cord).

NMR and MRI Protocols

Samples underwent NMR or MRI on 7T MRI scanners (Bruker, Germany). Spectroscopy measurements were performed on a horizontal-bore 7T scanner equipped with a Micro2.5 gradient insert having a maximal gradient strength of 1460 mT/m. Imaging measurements were performed on a vertical-bore 7T scanner having a nominal gradient strength of 400 mT/m.

AxCaliber NMR spectroscopy experiments included a series of pulsed gradient spin echo measurements with the following parameters: TR/TE = 3000/166 ms; $\delta = 2.5$ ms; $G_{max} = 1200$ mT/m; number of averages was 8; the diffusion time, Δ, was varied from 10 ms to 80 ms in eight increments (10, 15, 20, 30, 40, 50, 60, and 80 ms). Diffusion gradients were applied only perpendicular to the nerve axis with 16 increments in gradient amplitude per diffusion time. The entire DW dataset consisted of 128 spectra with a total duration of 51 min.

AxCaliber MRI experiments included a series of diffusion weighted stimulated echo imaging sequences with the following parameters: TR/TE = 3500/18 ms; $\delta = 4$ ms; $G_{max} = 300$ mT/m; number of averages = 6, with the diffusion time, Δ, chosen from 12 ms to 150 ms in five increments (12, 30, 60, 100, and 150 ms). Diffusion gradients were applied only perpendicular to the spinal cord axis with 16 increments in gradient amplitude per diffusion time. The imaging field of view was 12.8 mm^2 with matrix size of 96×64 (rebinned to 128×128) with a reconstructed image resolution of 100×100 μm. Images were taken from 10 consecutive axial slices with thickness of 4 mm and no gap between slices. The entire diffusion imaging dataset consisted of 80 images per slice that were acquired in 30 hr. In addition to the AxCaliber imaging experiments, a diffusion tensor imaging experiment was also performed using the stimulated echo diffusion-weighted imaging sequence with the following parameters: TR/TE = 6400/15 ms, $\Delta/\delta = 70/2.5$ ms, $G_{max} = 300$ mT/m measured at 15 noncollinear gradient directions. Twenty slices of 2 mm with no gap were imaged with field of view of 12.8 mm^2 with matrix of 96×64 (reconstructed to 128×128) with reconstructed image resolution of 100×100 μm, number of averages 6, with total experimental time of 11 hr.

AxCaliber Analysis

The following description of the AxCaliber analysis procedure was done similarly for the spectroscopy and imaging (analysis of the images was done on a pixel-by-pixel basis). AxCaliber analysis was done by extending the CHARMED approach described previously (36–37). In general, CHARMED combines contributions of hindered diffusion arising from the extra-axonal spaces and restricted diffusion arising from the intra-axonal spaces:

$$E(\mathbf{q},\Delta) = f_h \cdot E_h(\mathbf{q},\Delta) + f_r \cdot E_r(\mathbf{q},\Delta) \quad [1]$$

where $E(q,\Delta)$ is the observed diffusion signal decay, f_h is the hindered population fraction, E_h is the signal decay of the hindered diffusion fraction of water molecules, and f_r and E_r are the population fraction and signal decay of the restricted diffusion water molecules population.

Under the experimental protocol used in the AxCaliber framework (i.e., measuring the diffusion perpendicular to the fiber) the hindered diffusion surrounding the axons has Gaussian distribution and is thus modeled by the 1D Stejskal-Tanner equation:

$$E_h = \exp(-\gamma^2\delta^2 g^2 D_h(\Delta - \delta/3)) \quad [2]$$

where γ is the gyro-magnetic ratio, δ is the gradient duration, D_h is the hindered diffusion coefficient, and Δ is the diffusion time. In contrast to the hindered diffusion, the diffusion within the fibers can be modeled using different algorithms depending on the choice of experimental conditions (36,37). Since the experiments performed in this study satisfy the short gradient pulse approximation, we

used Callaghan's approach. The CHARMED expression for an axon with a radius a has the form:

$$E_r = \sum_k 4\ \exp[-\beta_{0k}^2 D_r \Delta / a^2] \times \left[\frac{(2\pi q a) J_0'(2\pi q a)}{(2\pi q a)^2 - \beta_{0k}^2}\right] + \sum_{nk} 8\ \exp[-\beta_{nk}^2 D_r \Delta / a^2] \times \frac{\beta_{nk}^2}{\beta_{nk}^2 - n^2} \times \left[\frac{(2\pi q a) J_n'(2\pi q a)}{(2\pi q a)^2 - \beta_{nk}^2}\right] \quad [3]$$

Where J'_n are the derivatives of the n^{th}-order Bessel function, β_{nk} are the arguments that result in zero-crossings; all other parameters have the above meanings. In our analysis routine n and k were incremented until their incremental contribution to the sum was negligible. Equation [3] models diffusion for a single fiber population; therefore, this formula was expanded to include contributions from a distribution of fiber diameters:

$$E_r = \sum_i \frac{f_i}{\pi a_i^2} \cdot \left[\sum_k 4\ \exp[-\beta_{0k}^2 D_r \Delta / a_i^2] \times \left[\frac{(2\pi q a_i) J_0'(2\pi q a_i)}{(2\pi q a_i)^2 - \beta_{0k}^2}\right] + \sum_{nk} 8\ \exp[-\beta_{nk}^2 D_r \Delta / a_i^2] \times \frac{\beta_{nk}^2}{\beta_{nk}^2 - n^2} \times \left[\frac{(2\pi q a_i) J_n'(2\pi q a_i)}{(2\pi q a_i)^2 - \beta_{nk}^2}\right]\right] \quad [4]$$

where f_i and a_i are the population fraction and corresponding axon radius, respectively; all other parameters have the above meaning. The weights of different axon diameters (w_i) were modeled by a gamma-function given by:

$$w_i(\alpha,\beta) = \frac{a_i^{\alpha-1} e^{-a/\beta}}{\beta^\alpha \Gamma(\alpha)} \quad [5]$$

In its final form, AxCaliber incorporates Eqs. 5, 4, and 2 into Eq. 1, where the diffusivity of hindered compartments, the population fraction, and the α and β parameters of the gamma function are fit simultaneously to all data points at all diffusion times using in-house MatLab (MathWorks, Natick, MA) code that employs a nonlinear least-square routine (utilizing Levenberg–Marquardt minimization). Initial conditions that limit the predicted diameter probability function were needed to obtain adequate convergence of the fitting routine.

Image Analysis

For the AxCaliber imaging the analysis resulted in a set of parameters (the diffusivities, the population fraction, and the Gamma function parameters). These parameters were used as an input for the multimodality image segmentation and clustering routine, previously described (38). Basically the routine creates a vector of parameters for each image pixel which then, following basic image analysis routine (histogram stretching and dimensionality reduction), undergoes clustering (using a modified k-means algorithm, see Ref. (38)). The same procedure was used for analysis of the immunohistochemistry stains of the spinal cord. Using this procedure we were able to perform automated cyto-architecture analysis and segment the spinal cord into different fascicles based on their myelin basic protein, oligodendrocytes, and general cell density. The AxCaliber imaging clustered image and the histology clustered image were than compared (see Results, Fig. 4).

Histology

Optic and Sciatic Nerve Preparations

Sciatic and optic nerves were cut to 1-mm^3 slices and fixed in 2.5% glutaraldehyde, osmificated, dehydrated with a graded series of ethanol and propylene oxide, and embedded in Araladite solution (Polysciences, Warrington, PA). Microsections (0.5 μm) were cut in an ultramicrotome (LKB, Sweden). Sections were collected over gelatin slides incubated with a 1% Toluidine blue stain for 1 min and examined using an optical microscope (Leica DMLS) for analysis.

Analysis of the axon diameter distribution of the electron microscope images was done using NIH Image (Bethesda, MD). This software identified the axons based on threshold segmentation. For each axon the diameter was estimated from its transverse area. Following this procedure a histogram of the diameter distribution was generated.

Spinal Cord Preparation

Spinal cords were fixed in 4% paraformaldehyde and left at 4°C for 48 hr. The spinal cords were divided into samples 1 cm long; each was dehydrated with a graded series of ethanol and xylene. Samples were embedded in paraffin blocks and cut in a microtome (Leica RM 2235). Then 10 μm sections were collected over gelatin slides. Deparaffinization was prepared/executed by xylene and ethanol subsequently sections were incubated 5 min in phosphate-buffered saline (PBS)×1, pH 7.4. Pretreatment for oligodendrocyte staining was performed in a boiled 10 mM citrate buffer pH 6.0 for 15 min and 20 min at room temperature. Slides were placed in an endogenous oxidation blocking solution (absolute methanol + 3% hydrogen peroxide) and rinsed 2 min in DDW and then 5 min in PBS×1. The blocking stage was made in Large Volume Ultra V Block (Lab Vision, Fremont, CA) 10 min at room temperature. Sections were incubated with primary antibody: oligodendrocyte Ab-2 (Mouse Monoclonal Antibody, Lab Vision/NeoMarkers) and Myelin Basic Protein Ab-1 (Rabbit Polyclonal Ab, Lab Vision/NeoMarkers) O.N at 4°C. The sections were incubated with Histofine (simple stain MAX PO multi Universal Immuno-peroxidase polymer, antimouse and rabbit, Nichirei Biosciences, Japan) for 30 min at room temperature. They were then rinsed twice with PBS×1 5 min. Finally, they were stained with Liquid DAB substrate kit (Zymed Laboratory, San Francisco, CA), histochemical substrate for horseradish peroxidase for 1 min, and washed 10 min in distilled water. The sections were dehydrated in 70, 95, 100% ethanol and xylene. Slides were then covered by mounting medium (Surgipath) and viewed under an optical microscope (Leica DMLS).

For the hematoxylin and eosin (H&E), staining slides were stained in hematoxylin (Harris Formula, Surgipath) 1 min, rinsed in running distilled water for 10 min, and

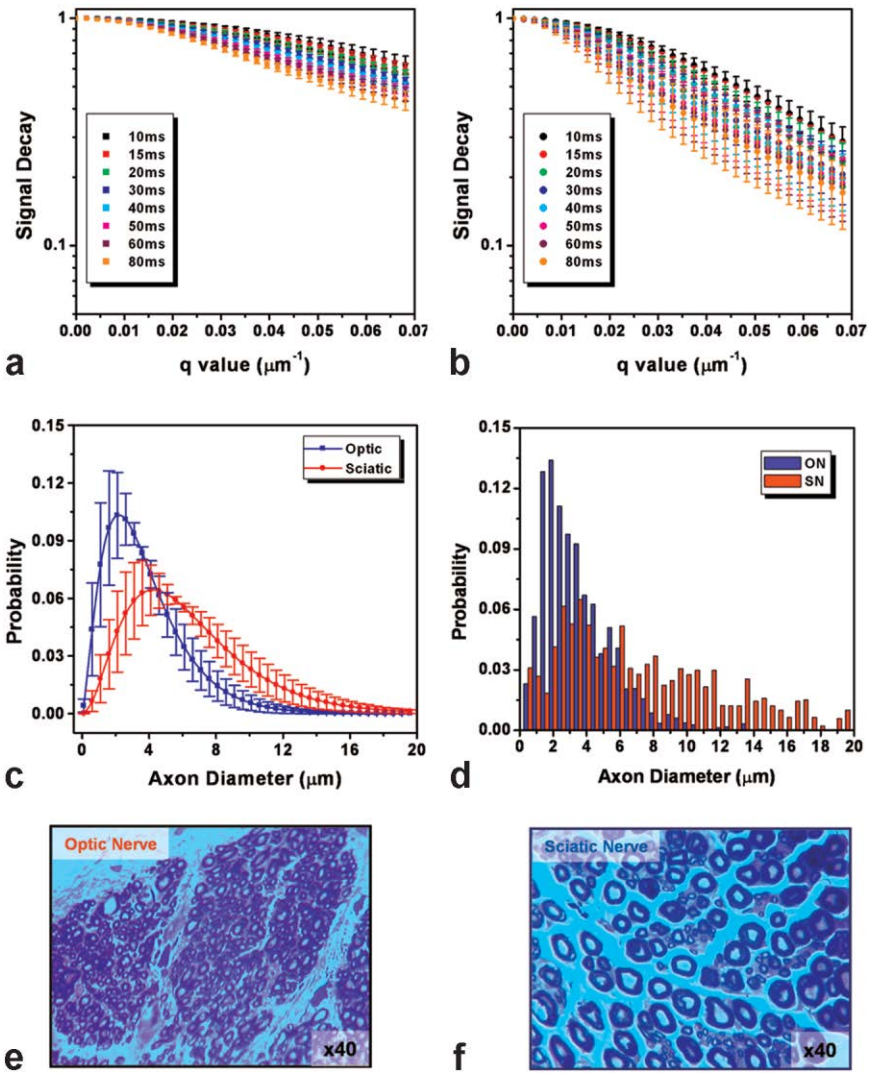

FIG. 1. AxCaliber of porcine optic and sciatic nerves. **a:** Multi diffusion time diffusion spectroscopy signal decay of an optic nerve sample. **b:** Multi diffusion time diffusion spectroscopy signal decay of a sciatic nerve sample. **c:** Extracted AxCaliber axon diameter distribution based on the signal decays given in **(a)** and **(b)**. **d:** Axon diameter distribution derived from electron microscopy section of the two nerve samples. **e,f:** Electron microscope section of one optic nerve **(e)** and one sciatic nerve samples upon which the data in **(a–d)** is based. Note the large difference in axonal morphometry between the two nerves.

then stained in eosin solution (Surgipath) for 1 min and washed again, dehydrated, and mounted.

RESULTS

AxCaliber of Sciatic and Optic Nerves

The signal decay vs. q data, measured over a range of different diffusion times, show significant differences between the optic and sciatic nerve specimen (Fig. 1a,b). First, the signal decay of the optic nerve is less attenuated than the sciatic nerve over the same range of q values. Second, the diffusion time dependence of the two tissues is different. While in the optic nerve the decay curves for different diffusion times are closely packed, in the sciatic nerve they are more spread out. These data suggest that the optic nerve has a large population of small-diameter axons exhibiting restricted diffusion even at the shortest diffusion time, whereas the sciatic nerve has a broader distribution of axon diameters in which not all axons exhibit restricted diffusion over the entire range of diffusion times. This is clearly what is seen in the histological data (see Fig. 1d). Figure 1c shows the axon diameter distribution curves as estimated using AxCaliber. As expected, the axon diameter curve for the optic nerve samples shows a narrow distribution centered around 3 μm (blue curve). In contrast, the sciatic nerve distribution is much broader, centered around 5–6 μm (red curve). Figure 1d shows the morphometric analysis from electron microscopy of histological sections of the two different nerves. Morphometric analysis shows the same pattern as AxCaliber: the optic nerve has a narrow distribution biased toward small axon diameters (0–4 μm) while the sciatic nerve has much broader distribution, with a larger number of large diameter axons (0–20 μm). The histological and MR-based axon diameter distributions were highly correlated for both nerves (with correlation coefficients of $r = 0.98$ for the optic nerve and $r = 0.86$ for the sciatic nerve). The means of the two measured axon diameter distributions were also similar; for the optic nerve the histological mean axon diameter was 3.48 μm while the AxCaliber mean diameter was 3.74 μm; for the sciatic nerve, the histological mean diameter was 7.3 μm while the AxCaliber mean diameter was 6.3 μm.

AxCaliber MRI of Porcine Spinal Cord

Figure 2 shows diffusion-weighted MR images and decays in different regions of the porcine spinal cord containing

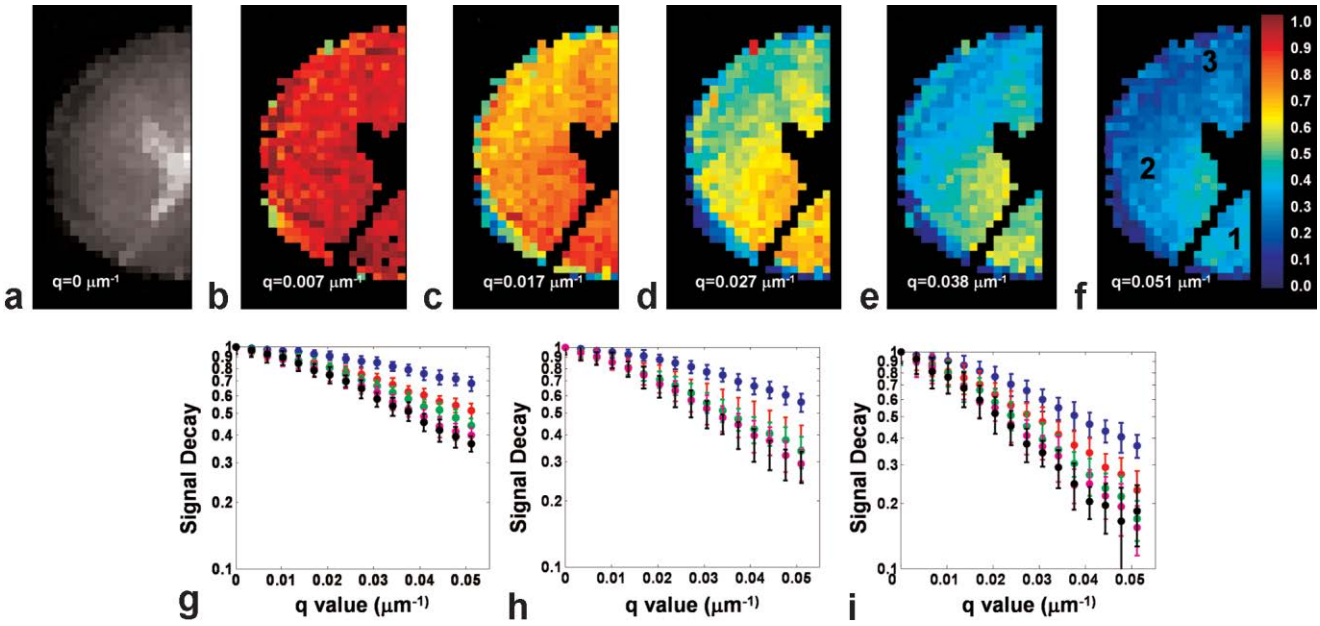

FIG. 2. AxCaliber MRI dataset of porcine spinal cord. **a:** Half spinal cord diffusion-weighted MRI with q = 0 representing the T_2 weighting of the sample. **b–f:** Diffusion-weighted images at different q values and diffusion time of 120 ms; all images are normalized to the q = 0 image (given in **a**), thus the color-scale represents the normalized decay. Note the differentiation to at least visual three regions in the most diffusion-weighted image. **f:** The fasciculus gracilis (dorsal region, 1), spinocerebellar and corticospinal fasciculi (lateral region, 2), and at the spinotectalis, reticulospinal, and vestibulospinal fasciculi (rostral region, 3). **g–i:** The corresponding diffusion signal decay from region of interest in the areas of the aforementioned regions with **(g)** corresponding to region 1, **(h)** to region 2, and **(i)** to region 3.

different white matter pathways. The areas are located at the fasciculus gracilis (rostral region), spinocerebellar and corticospinal fasciculi (lateral region), and at the spinotectalis, reticulospinal, and vestibulospinal fasciculi (rostral region). The diffusion time dependence and attenuation profile of the signals in these regions is significantly different, indicating different underlying morphology and microstructure of the white matter fibers. Note that the differences between the areas become more apparent as the q-value increases. These different diffusion time and signal decay behaviors are translated into different axon diameter distributions using AxCaliber on a pixel-by-pixel basis (AxCaliber MRI). To visualize the results of the AxCaliber imaging, we performed a cluster analysis (k-means, see Materials and Methods) on the free parameters estimated by AxCaliber (i.e., α and β of the Gamma distribution of axon diameters, their intra- and extra-axonal diffusivities and the intra-axonal volume fraction, see Materials and Methods). The seven distinct regions identified by the unsupervised 3D clustering algorithm across different slices of spinal cord white matter (Fig. 3) correlate well with the anatomical locations of the different fascicles (see below). The location of corresponding clusters was also similar across slices.

Comparison of AxCaliber MRI with Myelo-architectonic Analysis

Following MRI the spinal cords were histologically analyzed and then sectioned so that every third consecutive slice was stained with myelin basic protein (MBP), Oligodendrocyte (oligo-1), and H&E. Images of these stained sections were used as input for cyto-architecture digitized analysis (see Materials and Methods). The cyto-architectural analysis was able to segment the spinal cord into nine different regions with distinct MBP, oligo1, and H&E staining intensity, likely representing different white matter pathways (Fig. 4a), similar to textbook atlases. These nine regions were visually assigned to nine known white matter fascicles based on size, shape, and anatomical location. Visual inspection of the AxCaliber imaging segmentation (Fig. 4c) and the myelo-architecture segmentation (Fig. 4b) shows a close resemblance between the two, indicating that AxCaliber segmentation is indeed meaningful.

DISCUSSION

In this work we show that we can extract the diameter distribution of neuronal fibers from MRI data using a framework called AxCaliber. This allows one to measure microstructural and anatomical features of tissue, noninvasively and, potentially, in vivo, measurements which ordinarily could only be obtained using invasive histological methods. AxCaliber was demonstrated on porcine optic nerve, sciatic nerve, and spinal cord. In all cases we were able to compute the axon diameter distribution accurately and subsequently were able to use this estimated diameter distribution to segment tissue (similar to atlasing via cyto-architecture).

Another shortcoming of conventional histology is the need to examine small tissue sections, albeit at very high spatial resolution (< 1 μm). With AxCaliber, one can estimate microstructural features, like the axon diameter distribution, continuously throughout an entire brain. In this way both local and global spatial information can be ob-

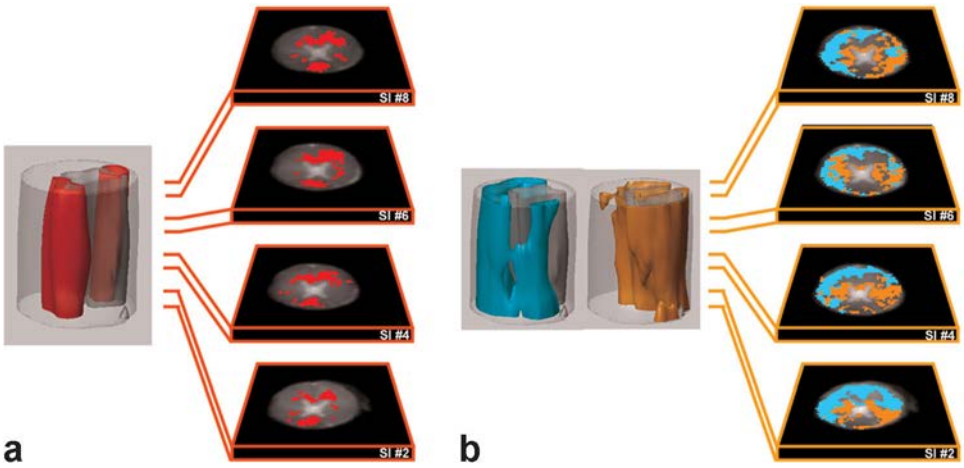

FIG. 3. 3D clusters of AxCaliber MRI of porcine spinal cord. **a:** Cluster 1 depicts mostly the dorsal fascicules gracilis. Note the similarity in the location of these regions along the spinal cord slices. **b:** Clusters 2 and 3 depict mostly the spinotectalis, reticulospinal, vestibulospinal fascicles (cyan) and the spinocerebellar and corticospinal fascicles (orange).

tained. Because the measurement is inherently noninvasive, it can also be performed longitudinally (on the same subject) or on different subjects, possibly using different scanners at different centers. This would allow for such population information to be obtained for the first time.

This information could have a significant impact on our understanding of white matter architecture and connectivity, neuroanatomical changes occurring in white matter disorders, and changes occurring in white matter during normal and abnormal development. In particular, AxCaliber can enhance connectivity studies since the presumption that the diameter distribution does not change along a fiber bundle from origin to target may be used to constrain the assessment of connectivity. For instance, AxCaliber would provide a means of testing hypotheses that the diameter distribution changes in diseases such as ALS and developmental disorders such as autism. AxCaliber also provides additional information for white matter tractography. One of the unresolved problems in tractography is how to follow fascicles in regions that are topologically complex, for example, at junctions where fibers cross or kiss (21). It is not possible using diffusion MR data alone to determine which of these architectural paradigms applies. If we make the reasonable assumption that the microarchitecture of fascicles remains continuous through such a junction, we can impose the continuity of the parameters characterizing the axon diameter distribution to determine which branches are connected through such a junction. Of course, this approach may fail in the optical chiasm, in which fibers from the same fascicles both cross and kiss, but we know of no other primary pathways in the brain where this complicated crossing pattern is known to occur normally.

Extracting the Diameter Distribution

AxCaliber takes a series of diffusion-weighted MR signals measured over a wide range of diffusion weightings (low and high b-values) and diffusion times. The key feature of this methodology is that at different diffusion times different populations of axons will exhibit restricted diffusion. So, by changing the diffusion time from short to long one can probe the relative contributions of different subpopulations of fibers. Specifically, in the short diffusion time limit the acquired diffusion signals are dominated by small axons exhibiting restricted diffusion, whereas in the long diffusion time limit most of the axons exhibit restricted diffusion. Using this approach the axon diameter

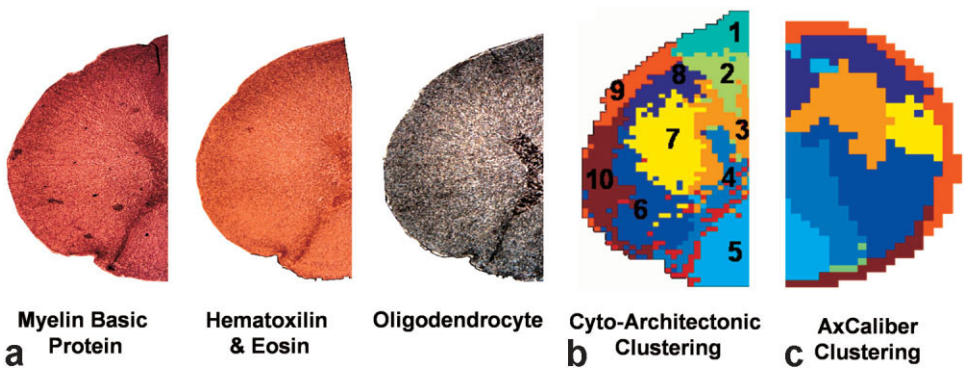

FIG. 4. Comparison of AxCaliber with histology. **a:** Histological staining of spinal cord section with MBP, cell body (H&E), and oligodendrocytes markers. **b:** Digitized cyto-architectonic analysis of the histological sections in **(a)** with the following fascicles identified: 1. Anterior spino-thalamic; 2. Reticulo-spinal; 3. Anterior cortico-spinal; 4. Gray matter; 5. Fasciculus gracilis and cuneatus; 6. Lateral cortico-spinal; 7. Lateral spino-thalamic; 8. Spino-tectalis; 9. Ventral spino-cerebellar; 10. Dorsal spino-cerebellar. **c:** AxCaliber clusters of the same spinal cord sections strongly resemble those obtained using histological analysis.

distribution can be modeled (quite reliably and stably) using a parametric probability function.

The magnitude of the maximum q-value used for AxCaliber will affect the estimate of the diameter distribution. The higher the q-value, the better the estimate of smaller axon diameters is. It is difficult to determine the q-value cutoff below which the estimation of the diameter distribution will be in error; most probably simulations can clarify this issue. The parameters used here (q_{max} = 0.07 μm^{-1}) allows adequate estimation of the diameter distribution. For the spinal cord, a smaller maximal q-value was used (0.05 μm^{-1}), which probably affects accuracy in the small diameter distribution region (<1 μm).

Tissue Segmentation

The axon diameter distribution is a morphological feature of the tissue. Different white matter fascicles often differ in the diameter distribution as well as in their myelin content, cell density, and other morphological features. To some extent these features are correlated with each other. For example, the axon diameter is correlated with the encapsulating myelin thickness (39). The comparison between myelo- and cyto-architectonic analysis in Fig. 4a,b and AxCaliber analysis (Fig. 4c) suggest that this correlation is indeed valid. As one goal of MRI-based anatomy studies is to parcellate the CNS into distinct regions, AxCaliber can provide an additional feature—the diameter distribution—to improve such segmentation. Although AxCaliber should be validated in more complicated white matter structures (e.g., in the brain), it should be noted that in the spinal cord such analysis is prone to errors. One artifact is rooted in the assumption that all fibers run perpendicular to the applied diffusion gradients. In the spinal cord there are some fiber populations that cross in the transverse plane, which the AxCaliber model does not account for. Implementing AxCaliber in 3D will solve this problem and make this methodology applicable to study the axon properties in brain white matter.

Model Assumptions, Limitations, and Experimental Considerations

The AxCaliber framework is based on two assumptions: 1) water diffusion within axons is restricted, and 2) the observed random displacements are perpendicular to the axon's main axis. The first assumption, while not proven, is supported by much circumstantial evidence. The thick lamellae of the myelin sheath surrounding axons provides a significant diffusion barrier to water over the timescales of a typical diffusion MR experiment. Therefore, it is reasonable to model the intra-axonal compartment of axons as a pack of impermeable cylinders containing water. The second condition of AxCaliber necessitates measuring water displacements perpendicular to the axis of the neuronal fibers. In the experiments using excised sciatic nerve, optic nerve, and spinal cord this condition is easily satisfied since we can align these samples accurately within the magnet. When the axons in a voxel are not coincident with the laboratory frame of reference, we can use DTI or CHARMED to determine the fiber axis prior to analyzing the data using AxCaliber.

While AxCaliber provides valuable information about tissue microstructure, it has some limitations both experimentally and computationally. First, AxCaliber requires the measurement of diffusion signal at multiple b or q values and multiple diffusion times, which can be costly in scanning time. This limits AxCaliber, in its current embodiment, from being used widely in vivo. Still, the information it provides even on in vitro samples is unique and cannot be obtained by histological methods on large-scale tissue sections. Second, AxCaliber is based on solving an inverse problem using differential weighting of contributions to the total signal arising from restricted diffusion at different diffusion times and gradient strengths. To that end it would be extremely helpful to acquire diffusion data using extremely short diffusion times (in which water diffusion appears Gaussian) to extremely long diffusion time (in which water diffusion is restricted and non-Gaussian). Of course, experimentally these extreme conditions cannot be met. Usually, the shortest possible diffusion time in research-orientated MRI scanners is currently about 10–20 ms; signal-to-noise limits the longest diffusion time we can sample. This constraint on short diffusion time obviously restricts accurate extraction of the diameter distribution of very small axons (<2 μm). For these types of tissues, even at the shortest diffusion time, diffusion within small axons is already restricted and extracting information regarding their weighting is prone to artifacts.

One computational issue relates to the function used to measure the axon diameter distribution. In the current implementation of AxCaliber we used a gamma-function to model the axon diameter distribution. In the cases we considered, this function provides a good fit to measured distribution. We also expect this function to work well in cases of healthy tissue, but it may fail when degenerative processes alter the distribution. For example, in ALS, where large diameter axons seem to be more damaged than smaller ones, or in experimental models of multiple sclerosis it is predicted that the distribution will be described by more complicated functions. For instance, electron microscopy of sciatic nerve exposed to allergic neuritis shows a multimodal diameter distribution that cannot be modeled by a single gamma distribution. To that end, the development of nonparametric approaches for estimation of the diameter distribution might overcome this limit. We have recently made some progress on this front (40).

Future Enhancements to AxCaliber

AxCaliber's current limitations, discussed above, will be addressed in several ways: 1) The experimental design will be optimized to reduce the number of diffusion-weighted signals required to estimate the axon diameter distribution adequately by using the minimal number of b values and diffusion times while maximizing model fidelity, accuracy, and precision; 2) The AxCaliber acquisition scheme will be extended to allow for the incorporation of diffusion-weighted data acquired in directions other than perpendicular to the fiber axis; 3) A nonparametric diameter distribution, rather than a parametric one, will be incorporated. This will be essential for in vivo applications, particularly when no a priori information about the

form of the underlying diameter distribution can be assumed.

ACKNOWLEDGMENT

The authors thank Liz Salak for editing the article.

REFERENCES

1. Hursh JB. The properties of growing nerve fibers. Am J Physiol 1939; 127:140–153.
2. Ritchie JM. On the relation between fibre diameter and conduction velocity in myelinated nerve fibres. Proc R Soc Lond B Biol Sci 1982; 217:29–35.
3. Waxman SG. Determinants of conduction velocity in myelinated nerve fibers. Muscle Nerve 1980;3:141–150.
4. Tasaki I, Ishii K, Ito H. On the relation between the conduction-rate, the fiber-diameter and the internodal distance of the medullated nerve fiber. Jpn J Med Sci III Biophys 1943;9:189–199.
5. Nicholls JG, Martin AR, Wallace BG, Fuchs PA. From neuron to brain. Sunderland, MA: Sinauer Associates; 2001.
6. Kandel ER, Schwartz JH, Jessell TM. Principles of neural science. New York: McGraw-Hill, Health Professions Division; 2000.
7. Salinas PC. Retrograde signalling at the synapse: a role for Wnt proteins. Biochem Soc Trans 2005;33(Pt 6):1295–1298.
8. Cluskey S, Ramsden DB. Mechanisms of neurodegeneration in amyotrophic lateral sclerosis. Mol Pathol 2001;54:386–392.
9. Heads T, Pollock M, Robertson A, Sutherland WH, Allpress S. Sensory nerve pathology in amyotrophic lateral sclerosis. Acta Neuropathol (Berl) 1991;82:316–320.
10. Piven J, Bailey J, Ranson BJ, Arndt S. An MRI study of the corpus callosum in autism. Am J Psychiatry 1997;154:1051–1056.
11. Basser PJ. Inferring microstructural features and the physiological state of tissues from diffusion-weighted images. NMR Biomed 1995;8:333–344.
12. Basser PJ, Jones DK. Diffusion-tensor MRI: theory, experimental design and data analysis—a technical review. NMR Biomed 2002;15:456–467.
13. Basser PJ, Mattiello J, LeBihan D. MR diffusion tensor spectroscopy and imaging. Biophys J 1994;66:259–267.
14. Basser PJ, Pierpaoli C. A simplified method to measure the diffusion tensor from seven MR images. Magn Reson Med 1998;39:928–934.
15. Le Bihan D. Diffusion and perfusion magnetic resonance imaging: applications to functional MRI. New York: Raven Press; 1995.
16. Moseley ME, Cohen Y, Kucharczyk J, Mintorovitch J, Asgari HS, Wendland MF, Tsuruda J, Norman D. Diffusion-weighted MR imaging of anisotropic water diffusion in cat central nervous system. Radiology 1990;176:439–445.
17. Pajevic S, Pierpaoli C. Color schemes to represent the orientation of anisotropic tissues from diffusion tensor data: application to white matter fiber tract mapping in the human brain. Magn Reson Med 2000;43:921.
18. Pierpaoli C, Jezzard P, Basser PJ, Barnett A, Di Chiro G. Diffusion tensor MR imaging of the human brain. Radiology 1996;201:637–648.
19. Pierpaoli C, Basser PJ. Toward a quantitative assessment of diffusion anisotropy. Magn Reson Med 1996;36:893–906.
20. Beaulieu C, Allen PS. Determinants of anisotropic water diffusion in nerves. Magn Reson Med 1994;31:394–400.
21. Basser PJ, Pajevic S, Pierpaoli C, Duda J, Aldroubi A. In vivo fiber tractography using DT-MRI data. Magn Reson Med 2000;44:625–632.
22. Catani M, Howard RJ, Pajevic S, Jones DK. Virtual in vivo interactive dissection of white matter fasciculi in the human brain. Neuroimage 2002;17:77–94.
23. Conturo TE, Lori NF, Cull TS, Akbudak E, Snyder AZ, Shimony JS, McKinstry RC, Burton H, Raichle ME. Tracking neuronal fiber pathways in the living human brain. Proc Natl Acad Sci U S A 1999;96: 10422–10427.
24. Mori S, Crain BJ, Chacko VP, van Zijl PC. Three-dimensional tracking of axonal projections in the brain by magnetic resonance imaging. Ann Neurol 1999;45:265–269.
25. Mori S. MRI atlas of human white matter. Amsterdam: Elsevier; 2005.
26. Stejskal EO, Tanner JE. Spin diffusion measurements—spin echoes in presence of a time-dependent field gradient. J Chem Phys 1965;42:288–292.
27. Callaghan PT. Principles of nuclear magnetic resonance microscopy. Oxford: Clarendon Press; New York: Oxford University Press; 1991.
28. Assaf Y, Ben-Bashat D, Chapman J, Peled S, Biton IE, Kafri M, Segev Y, Hendler T, Korczyn AD, Graif M, Cohen Y. High b-value q-space analyzed diffusion-weighted MRI: application to multiple sclerosis. Magn Reson Med 2002;47:115–126.
29. Assaf Y, Mayk A, Cohen Y. Displacement imaging of spinal cord using q-space diffusion-weighted MRI. Magn Reson Med 2000;44:713–722.
30. Cory DG, Garroway AN. Measurement of translational displacement probabilities by NMR—an indicator of compartmentation. Magn Reson Med 1990;14:435–444.
31. Callaghan PT, Coy A, Macgowan D, Packer KJ, Zelaya FO. Diffraction-like effects in NMR diffusion studies of fluids in porous solids. Nature 1991;351:467–469.
32. Packer KJ, Rees C. Pulsed NMR studies of restricted diffusion. 1. Droplet size distributions in emulsions. J Colloid Interface Sci 1972;40:206–218.
33. Callaghan PT, Jolley KW, Humphrey RS. Diffusion of fat and water in cheese as studied by pulsed field gradient nuclear magnetic-resonance. J Colloid Interface Sci 1983;93:521–529.
34. van den Enden JC, Waddington D, van Aalst H, van Kralingen CG, Packer KJ. Rapid-determination of water droplet size distributions by PFG-NMR. J Colloid Interface Sci 1990;140:105–113.
35. Hollingsworth KG, Johns ML. Measurement of emulsion droplet sizes using PFG NMR and regularization methods. J Colloid Interface Sci 2003;258:383–389.
36. Assaf Y, Freidlin RZ, Rohde GK, Basser PJ. New modeling and experimental framework to characterize hindered and restricted water diffusion in brain white matter. Magn Reson Med 2004;52:965–978.
37. Assaf Y, Basser PJ. Composite hindered and restricted model of diffusion (CHARMED) MR imaging of the human brain. Neuroimage 2005; 27:48–58.
38. Yovel Y, Assaf Y. Virtual definition of neuronal tissue by cluster analysis of multi-parametric imaging (virtual-dot-com imaging). Neuroimage 2007;35:58–69.
39. Waxman SG, Kocsis JD, Stys PK. The axon: structure, function, and pathophysiology. New York: Oxford University Press; 1995.
40. Assaf Y, Blumenfeld, T, Levin, G, Yovel, Y, Basser, PJ. AxCaliber—a method to measure the axon diameter distribution and density in neuronal tissues. Proc Intl Soc Magn Reson Med 2006;14:637.